

Electron and Phonon Confinement and Surface Phonon Modes in CdSe-CdS Core-Shell Nanocrystals

A . Singha^y, B . Satpati^z, P.V . Satyam^z and Anushree Roy^y

^yDepartment of Physics, Indian Institute of Technology, Kharagpur 721 302, W B , India

^zInstitute of Physics, Bhubaneswar 751005, India

Abstract

Optical and vibrational properties of bare and CdS shelled CdSe nanocrystalline particles are investigated. To confirm the formation of such nanocrystals in our samples we estimate their average particle sizes and size distributions using TEM measurements. From the line profile analysis of the images the core-shell structure in the particles has been confirmed. The blue shift in optical absorption spectra, analyzed using theoretical estimates based on the effective bond order model, establishes the electron confinement in the nanoparticles. Unique characteristics of the nanocrystals (which are absent in the corresponding bulk material), such as confinement of optical phonons and the appearance of surface phonons, are then discussed. Making use of the dielectric response function model we are able to match the experimental and theoretical values of the frequencies of the surface phonons. We believe that our studies using optical probes provide further evidence on the existence of core-shell structures in CdSe-CdS type materials.

Electronic address: anushree@phy.iitkgp.ac.in

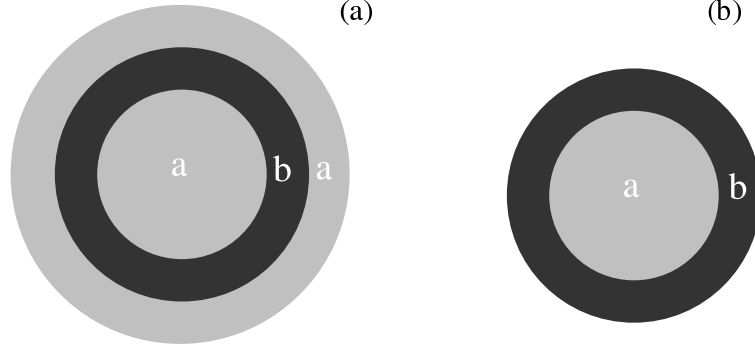


FIG. 1: Schematic drawing of the nano-onion and core-shell type nanoparticles

I. INTRODUCTION

Over last couple of decades, unique physical properties due to quantum confinement effects have been reported for a wide range of semiconductor nanocrystalline materials [1]. Since in these systems surface to volume ratio is high compared to that of corresponding bulk materials, surface states play a crucial role in determining their physical properties. The surface of nanocrystals is made of atoms that are not fully coordinated. Hence, they are highly active and these surface atoms act like defect states unless they are passivated by either organic ligands or higher bandgap semiconductor materials [1, 2]. Thus, the current direction in this field of research includes modification of given size-quantized semiconductor particles by means of surface chemistry. In the literature, we find reports on quantum dot-quantum well (QDQW) and core-shell nanocrystalline structures due to surface modifications of the particles. QDQW is a three layered structure consisting of a size quantized particle acting as a core [marked 'a' in Fig. 1 (a)] and a complete layer of another material on the surface [marked 'b' in Fig. 1 (a)] of this core, which is again covered by core material as an outermost shell. This core-shell-core structure is marked as a-b-a in Fig. 1 (a). Colloquially, these particular structures are also called 'nano-onions'. Recently, Dorfs and Eychmüller have outlined the preparation and characterization of a series of QDQW systems containing two wells [3]. Coating nanoparticles by another material yields core-shell nanocrystals [see Fig. 1 (b)] [1].

In core-shell structure, like inorganic epitaxial shell growth, the organic ligands cannot passivate both cationic and anionic surface sites of the core [4]. The particles passivated by

inorganic shell structures are more robust than organically passivated nanocrystals and have greater tolerance to processing conditions necessary for incorporation into solid structures [5]. For effective surface passivation, the core particles having certain band gap are capped with a higher band gap material. Moreover, the conduction band energy of the capping (shell) material is usually higher than that of the core material with the valence band energy of the capping material being lower. This energetic situation is called a type-I structure [1]. Due to presence of higher band gap capping material, the photogenerated excitons in the core remain localized in the same region and are forced to recombine while spatially confined in the core. Confinement of electrons in the nanocrystals gives rise to blue shift in optical absorption and PL spectra of the material. As the non-radiative decay channels through surface states are not accessible for these electrons, core-shell structures thus formed show higher luminescence quantum yields [2, 4, 6, 7, 8, 9, 10, 11] lower fluorescence life time [10] and many other benefits [12] related to tuning of band gap in two materials.

Like electrons, phonons are also confined in nanocrystals. In bulk crystals, the phonon eigenstate is a plane wave and wavevector selection rule for the first order Raman scattering requires $q \neq 0$. In contrast, the spatial correlation function of the phonon becomes finite due to its confinement in the nanocrystal and hence the $q \neq 0$ selection rule gets relaxed. In general, the phonon-dispersion curves of bulk crystals show the frequency ω to be a decreasing function of wavevector q . Hence, the first order Raman line shifts and broadens towards the low frequency side for the nanocrystals. This has been proposed and explained by phonon confinement model [13]. Confinement of phonons for Si, Ge, BN, CdS, CdS_xSe_{1-x} and many other nanocrystals have been reported in the literature [14, 15, 16, 17, 18, 19].

As mentioned before, surface states play an important role in deciding different physical properties of nanocrystals. For a plane wave propagating in the x-direction in a bulk crystal, the temporal and spatial variation of the wave is described by the factor $\exp[i(kx - \omega t)]$, where the wavevector $k = \frac{\omega}{v} = \frac{\omega}{c} \sqrt{\epsilon}$; ϵ is the dielectric constant of the crystal. In the frequency range between bulk longitudinal optical (LO) phonon frequency, ω_{LO} , and transverse optical (TO) mode frequency, ω_{TO} , $\epsilon < 0$, k is imaginary. Therefore, in this frequency range the wave decays exponentially in the medium, i.e. it can not propagate in bulk crystals and only surface modes exist [20]. Because of enhanced surface to volume ratio these modes appear for nanocrystals and it provides relevant information on surface states. Recently, Baranov et al have reported the surface phonon modes in ZnS shelled CdSe

particles [21].

Characteristics of bare CdSe nanocrystals are now well established. CdSe nanocrystals passivated with long organic chain (like TOPO) have room temperature photoluminescence (PL) (quantum yield 10%) with very long fluorescence time [22, 23]. The inorganic shelling of CdSe core by CdS has also been explored and shown to be better for surface passivation. Previous HRTEM and XPS measurements have shown that shell growth in this system does not form an alloy [4, 24]. The lattice mismatch of 3.9% between CdS and CdSe is small enough to allow epitaxial growth while still preventing alloying. Moreover, the difference in band gap (2.42 eV for CdS and 1.74 eV for CdSe at room temperature) is large enough for shell growth. The room temperature PL yield for CdSe-CdS core-shell system has been reported to be up to 50% [4]. The electronic structure in this material can be understood from molecular orbital model and particle in a box model, as discussed in Ref. [4]. The same has also been discussed from the analysis of photoelectron spectra from core-shell structure [24]. The high photostability of the system has been explained by confinement of electrons and holes in the core-shell region.

In this article, we have discussed the optical properties of mercaptoacetic acid stabilized bare CdSe particles and CdS capped CdSe particles. The nanoparticles have been characterized by their absorption spectra as well as by high resolution transmission electron microscope (HRTEM) images. The optical transition is modeled using Effective bond order model (EBOM). Average particle size and size distribution of the particles have been estimated from both HRTEM images and optical absorption measurements; which have been further supported by Raman measurements. We have quantitatively analyzed asymmetric Raman line shapes including both confined optic modes and surface phonon modes. The observed frequencies of the SP modes in these systems have been compared with the calculations based on the dielectric response function model. In Section II of this article, we have briefly discussed the sample preparation procedure, which we have followed. Section III deals with analysis of HRTEM images of the samples. Section IV demonstrates the optical properties of the samples, studied by optical absorption and PL spectroscopy. Detail analysis of phonon spectra is reported in Section V. Finally, in section VI, we have summarized our results with a few concluding remarks.

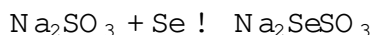
II. SAMPLE PREPARATION

A. Chemicals

For sample preparation, Cadmium perchlorate, $[Cd(ClO_4)_2]$ and Mercaptoacetic acid $[HS-CH_2-COOH]$ were purchased from Aldrich, USA and LOBA Chemie, India respectively. Anhydrous Sodium sulfate $[Na_2SO_3]$ and Sodium sulfide $[Na_2S]$ were from MERCK Ltd., India and S.D. Fine Chem. LTD., India respectively. Solid Selenium powder $[Se]$ and Sodium hydroxide $[NaOH]$ were used as received.

B. Preparation of stock solution of Na_2SeSO_3

1.0 gm of Se powder was added in 200 ml (1.1 M) hot Na_2SO_3 solution under stirring condition and then boiled for half an hour. Subsequently, the solution was cooled at room temperature and the aqueous layer was filtered using Whatman filter paper. This solution is used as the stock solution.



C. Preparation of mercaptoacetic acid stabilized CdSe nanocrystals : Sample A

Following Liu et al [25], 150 ml of $Cd(ClO_4)_2$ (2×10^{-4} M) and 150 ml of $HS-CH_2-COOH$ (2×10^{-4} M) were mixed and stirred vigorously for about 5 min. Here, the latter acts as a stabilizing agent. The pH of the solution was adjusted to 9.0 by adding aqueous $NaOH$ (1.0 M) solution and heated to $100^\circ C$ under N_2 atmosphere. Subsequently, 0.5 ml of Na_2SeSO_3 was added drop wise to the solution and boiled again for about half an hour under stirring condition. The solution turned orange in color indicating the formation of CdSe particles.

D. Preparation of mercaptoacetic acid stabilized CdSe-CdS core-shell nanocrystals: Sample B

For the preparation of coated CdSe-CdS particle, the above CdSe solution was cooled to $50^\circ C$ and 20 ml of $Cd(ClO_4)_2$ (0.1M) and 20 ml of Na_2S (0.1M) were added drop wise alternatively under stirring condition in N_2 atmosphere. After 30 min of stirring the solution

turned orange-red in color due to formation of CdSe-CdS core-shell particles.

III. AVERAGE PARTICLE SIZE AND SIZE DISTRIBUTION : HRTEM

Samples for Transmission Electron Microscopy were deposited onto 300 mesh copper TEM grids coated with 50 nm carbon film. Samples A and B are suspended in water; thus, directly added drop-wise on the grid. The excess water was allowed to evaporate in air. The grids were examined in JEOL 2010 microscope with Ultra-High Resolution (UHR) microscope using a LaB₆ filament operated at 200 kV. HRTEM images of many nanocrystals for each sample were measured and analyzed.

TEM has been used to determine the particle size and size distribution of the aforementioned nanocrystals. Also, using the high resolution TEM, it is possible to confirm the core-shell structure of nanocrystals [4]. Low magnification TEM micrographs are shown in Fig. 2 (a) and (c) for Sample A and B, respectively. Fig. 2 (b) and (d) are the histogram plots, obtained by measuring sizes of many particles per sample. Size distribution for the nanoparticles are usually found to be log-normal:

$$P(d) = \frac{1}{\sigma \sqrt{2\pi}} \exp \left(-\frac{(\ln(d/d_0))^2}{2\sigma^2} \right) \quad (1)$$

Here d is the average size and σ is related to the size distribution of the particles. By fitting the frequency plot using Eqn. 1 (solid lines in Fig. 2), we have estimated the average particle size (d) and σ of the particles, which are listed in Table I. The size distribution of the particles is estimated to be more spread out for bare particles (Sample A) compared to the other sample.

Transmission electron microscopy measurements provide the convincing proof of the crystalline core-shell structure of the sample. Fig. 3 shows high resolution micrograph of selected nanocrystals along the line profiles. The contrast in the image depends on the electron density in the object forming the image. Hence, CdS is expected to show less contrast than CdSe since the former has fewer electrons per unit cell. The line profile of the image contrast for Sample A and B corresponding to the images are presented in Fig. 3 (b) and (d). For Sample A, we observe a smooth drop in the contrast near the edge of the nanocrystal. In comparison, the line profile of core-shell nanocrystals (Sample B), exhibit a trend of a stepwise-drop. The contrast can also be explained by the change in thickness of nanocrystals,

Sam ple	TEM		O A S		R am an
	d nm		d		d
Sam ple A	5.2	0.22	6.0	0.22	4.7
Sam ple B	5.4	0.11	7.0	0.11	5.0

TABLE I: Comparison of the average size and size distribution of the particles in Sample A and B as obtained from blue shift in TEM images, optical absorption bands and content of phonons

Sam ple	B and I nm (eV)	B and II nm (eV)	PL peak nm (eV)
Sam ple A	577 (2.15)	–	538 (2.31)
Sam ple B	606 (2.05)	477 (2.60)	541 (2.29)

TABLE II: (a) Optical absorption and PL bands for Sample A and Sample B

but it is not very probable that it would occur in such a step-like way. From the HRTEM images the average shell thickness of the particles in Sample B has been estimated to be 1.2 nm.

From the micrograph [Fig. 3 a], we have determined the lattice spacing in Sample A to be 3.72 Å, which corresponds to (100) plane of CdSe in hexagonal phase [26].

IV. OPTICAL PROPERTIES OF NANOCRYSTALLINE PARTICLES

A. Electron content : Optical absorption spectroscopy

Fig. 4 (a) shows the optical-absorption spectra for the samples A and B. The absorption band energy (wavelength) from these samples are tabulated in Table II. The bulk band gaps for CdSe and CdS at room temperature are 1.74 eV and 2.42 eV, respectively. Samples A (CdSe particles) show only Band I at 2.15 eV in optical absorption spectrum (see Table II). We have observed that due to CdS shell growth a new band (Band II) at 2.60 eV appears in the optical absorption spectrum in addition to Band I.

The blueshift in the optical absorption spectra of the particle from that for bulk CdSe and CdS arises from the content of charge carriers in the nanocrystals. Assuming the particles to be spherical, the optical-absorption coefficient of the collection of the monodispersed particles of average diameter d at low temperature is given by

	Electronic transition	Con nement energy (ev)	Type	f_i	A_i	x_i
CdSe	$1_{8^{-}}-1_{6^{+}}$	0.42	1	4.85	55.50	1.23
	$1_{6^{+}}-1_{7^{-}}$	0.83	2	1.11	38.71	0.99
	$1_{6^{+}}-1_{8^{-}}$	0.84	2	0.10	38.71	0.99
	$2_{7^{-}}-1_{6^{+}}$	0.72	3	0.61	70.35	1.17
	$2_{8^{+}}-1_{8^{-}}$	0.75	3	1.89	70.35	1.17
	$1_{7^{+}}-1_{8^{-}}$	0.78	3	0.62	70.35	1.17
	$3_{7^{-}}-1_{6^{+}}$	0.76	3	0.01	70.35	1.17
CdS	$1_{8^{-}}-1_{6^{+}}$	0.40	4	4.13	45.40	1.19
	$1_{7^{-}}-1_{6^{+}}$	0.45	4	1.73	45.40	1.19

TABLE III: The con nement energy, E , changes with diam eter of the particle d by follow ing the relation $E = A_i d^{-X_i}$; where E is in eV and d in Å

$$(E) = \sum_i \frac{f_{i,i}}{(E - E_i)^2 + \frac{\gamma_i^2}{4}}; \quad (2)$$

where, f_i is the oscillator strength, E_i is the transition frequency and γ_i is the half width at half maximum (HWHM) for the i th interband transition. Due to thermal broadening and inhomogeneous broadening due to size distribution of the particles Eqn. 2 is modified to

$$_{\text{observed}}(E) = B \sum_i \int_0^\infty d(d) \frac{P(d) f_{i,i}}{[E - E_i(d)]^2 + \frac{\gamma_i^2}{4}}; \quad (3)$$

where $P(d)$ is the log-normal size distribution of the particles, same as Eqn.1. The results of single band effective mass approximation model do not agree with the optical absorption spectra of the nanocrystals because it neglects intervalence band mixing and deviation from quadratic dispersion. This has been shown in the literature for bare CdSe or CdS particles and CdS-CdSe mixed crystals [19, 27]. We have assumed results from effective bond order model by Ramaniyah and Nair on interband transition in quantum dots of CdS and CdSe and considered the following transitions: $1_{8^{-}}-1_{6^{+}}, 1_{6^{+}}-1_{7^{-}}, 1_{6^{+}}-1_{8^{-}}, 2_{7^{-}}-1_{6^{+}}, 2_{8^{+}}-1_{8^{-}}, 1_{7^{+}}-1_{8^{-}}, 3_{7^{-}}-1_{6^{+}}$, for CdSe core $1_{8^{-}}-1_{6^{+}}, 1_{7^{-}}-1_{6^{+}}$ for CdS shell [27]. Con nement energies for these transitions as obtained in Ref. [27] are tabulated in Table III. We have grouped these transitions in 3 types for CdSe and 1 type for CdS, according to their con nement energies. Since the oscillator strength is not very sensitive to particle diameter d [2, 3]

nm, the value of f_i corresponds to those of $d = 4.8$ nm for transitions in CdS and $d = 4.6$ nm for CdSe as obtained in Ref. [27]. The con nement energy (E) for these 4 types of transitions vs: particle size have been plotted in Fig. 5. For (E) we have assumed the empirical relation [19]

$$(E) = A_i d^{x_i}; \quad (4)$$

where A_i and x_i are constants for a particular transition. We have tted the 4 types of transitions with Eqn.4 (shown in Fig. 5) and estimated the values of A_i and x_i for these transitions, which are given in Table III. Taking $E_i(d) = E_g^{\text{bulk}} + A_i d^{x_i}$ we have tted the experimental optical absorption spectra, shown by dashed-dotted lines in Fig 4 (b) and (c) for Sample A and B, respectively. It can be seen that the theoretical curves t the experimental data reasonably well. The values of average particle size and from the above analysis are tabulated in Table I. The same Table also reveals the comparison between the average sizes of the particles obtained from optical absorption measurements and HRTEM frequency plots.

B. Photoluminescence

Photoluminescence spectra is obtained using 1200 g/mm holographic grating, a holographic super notch filter, and a Peltier cooled CCD detector. Spectra are taken using 488 nm Argon ion laser as an excitation source.

Figure 6 shows the PL spectra from the Samples A and B. The PL peak positions, obtained by tting each spectrum by a Gaussian distribution have been tabulated in Table II. PL peaks from all the samples are slightly blue or red shifted from the rst excitonic peak in the absorption spectra. This shift results from the convolution of the size distribution and the emitting state and excitation energy for the excitation near the rst peak [23, 28]. The detail study on the photo-stability of the particles, prepared exactly by the same route, has been reported in Ref [25].

V. CONFINEMENT OF OPTIC PHONON AND NEW SURFACE PHONONS RAMAN SCATTERING

In order to understand the nature of phonon confinement and appearance of new surface modes in our samples, we have performed Raman scattering studies. Raman spectra are obtained using the same experimental set up as used for the above mentioned PL measurements. The slit width of the spectrometer during the experiment was 50 μm . The first order Raman spectra for the samples are shown in Fig. 7. Using the phonon confinement model of Campbell and Fauchet [13], the first order Raman spectrum $I_c(\omega)$ is given by

$$I_c^j(\omega) = A \int_0^{q_{\text{max}}} \frac{dq \mathcal{C}^j(0; q)}{[\omega - \omega_j(q)]^2 + (\gamma_j/2)^2}; \quad (5)$$

where $\omega_j(q)$ and γ_j are the phonon dispersion curve and the natural line width (FWHM) of the corresponding bulk materials, $\mathcal{C}^j(0; q)$ is the Fourier coefficient of the phonon confinement function. A is an arbitrary constant. $j=1$ for CdS and $j=2$ for CdSe. For nanoparticles, it has been shown that the phonon confinement function, which fits the experimental data best, is $W(r; d_z) = \exp(-\frac{8}{d_z^2} r^2)$, the square of the Fourier coefficient of which is given by $\mathcal{C}^j(0; q)^2 = \exp(-\frac{q_z^2 d_z^2}{16})$. Here, d_1 is the average size of the spherical nanocrystals in Sample A and d_2 is the average diameter of the core in Sample B. On the other hand, for the shell component of particles in core-shell structure (Sample B), we have used an additional phonon confinement function for CdS shell, given by [13]

$$\mathcal{C}^j(0; q)^2 = \exp\left(-\frac{q_1^2 t^2}{16}\right) \left[1 - \text{erf}\left(\frac{q_1 t}{32}\right)\right]^2 \quad (6)$$

where t is the average shell thickness for the particles. The average phonon dispersion in the bulk CdSe and CdS crystal for the LO phonon modes are taken as [29, 30]

$$\omega_j(q) = \omega_0^j + \alpha_j^2 q^2 \quad (7)$$

which fits the experimental curve well in the direction of Γ -M upto $q_{\text{max}} = 0.4$. ω_0^j is the corresponding bulk LO phonon frequency: $\omega_0^1 = 302 \text{ cm}^{-1}$ and $\omega_0^2 = 213 \text{ cm}^{-1}$. α_j^2 is the band width of bulk LO phonon branch: $\alpha_1^2 = 102 \text{ cm}^{-1}$, $\alpha_2^2 = 118 \text{ cm}^{-1}$. In the above equations, q_j is taken in unit of $2\pi/a_j$, where, a_j is the lattice constant of the material. We have taken $a_1 = 5.82 \text{ \AA}$ and $a_2 = 6.08 \text{ \AA}$ [26].

In addition to LO phonon peak, we have also observed additional peaks in the spectra for Sample A and B. Keeping in mind the possibility of the presence of the surface phonons (SP) between longitudinal and transverse optical phonon modes, together with the confined optical phonon, we have fitted this additional peak with the Lorentzian function

$$I_{SP}^j(\omega) = \frac{B_{SP}}{(\omega - \omega_{SP})^2 + \frac{\Gamma_{SP}^2}{4}}; \quad (8)$$

where ω_{SP} and Γ_{SP} are the peak position and the HWHM, respectively, for the SP mode. We fit the full spectrum for Sample A and B by a combined line shape $I(\omega) = I_c^j(\omega) + I_{SP}^j(\omega)$. The best fit obtained for both the samples are shown by the solid lines in Fig. 7. The phonon confinement components are shown by dashed lines and the surface phonon components are shown by dotted lines in Fig. 7. In the fitting procedure, we have kept d_z , t , ω_{SP} , Γ_{SP} , A and B as fitting parameters. For the best fit of the spectra the values of $\omega_0=2$ for Sample A and Sample B are taken to be 32 cm^{-1} and 14.5 cm^{-1} . We attribute the variation in the value of $\omega_0=2$ from sample to sample to the difference in size distribution of the particles. From the non-linear least square fit, the average particle size (d_1) for Sample A is obtained as 4.7 nm . The core diameter (d_2) and shell (In) thickness, t , for Sample B are obtained as 4.0 nm and 1.25 nm . This estimates average particle diameter ($d_2 + t$) in Sample B to be 5.25 nm . The diameters of the particles in Sample A and B thus measured are very close to the same estimated from optical absorption and HRTEM measurements [see Table I]. We have observed that the SP modes for Sample A at 183 cm^{-1} and for CdSe and CdS-like modes in Sample B at 180 cm^{-1} and 244 cm^{-1} , respectively. The ratio of A/B is 2×10^3 for Sample A, whereas, the ratio of the same for CdS-like and CdSe-like modes in sample B are 85 and 68.

For core-shell nanocrystals, we have considered the optical modes as the response of the two types of oscillators under applied electric fields. The effective oscillator strength is proportional to the density of the oscillators. Assuming nonoverlapping reststrahlen bands for these two modes $\omega_{LO1} > \omega_{TO1} > \omega_{LO2} > \omega_{TO2}$, the dielectric response function of a core-shell particle can be taken as [19]

$$\epsilon(\omega) = p_1 \epsilon_1(\omega) + (1 - p) \epsilon_2(\omega) \quad (9)$$

where $\epsilon_1(\omega)$ and $\epsilon_2(\omega)$ are given by

$$\omega_j^2 = \omega_1^2 + \frac{\omega_{LOj}^2 - \omega_{TOj}^2}{\omega_{TOj}^2} \quad (10)$$

and ϵ_1 is the high frequency dielectric constant of the crystal. Here, we have taken $p = t/(t+x)$, where t is the CdS shell thickness, as taken earlier and x is the depth of penetration of the surface phonon within the CdSe core region of the core-shell structure. Substituting Eqn. 10 in Eqn. 9 for both CdS and CdSe like modes and using $\omega_j^2 = (\omega_j^2 + \omega_1^2)/2$ [20], we get the following equation for the surface phonon frequencies of the core-shell nanocrystals:

$$\omega_j^4 - \omega_j^2 \left(\omega_{TO1}^2 + \omega_{TO2}^2 + \frac{p}{K} (\omega_{LO1}^2 - \omega_{TO1}^2) + \frac{(1-p)}{K} (\omega_{LO2}^2 - \omega_{TO2}^2) \right) + \omega_{TO1}^2 \omega_{TO2}^2 \left(1 + \frac{p}{K} \frac{(\omega_{LO1}^2 - \omega_{TO1}^2)}{\omega_{TO1}^2} + \frac{(1-p)}{K} \frac{(\omega_{LO2}^2 - \omega_{TO2}^2)}{\omega_{TO2}^2} \right) = 0 \quad (11)$$

Here, $K = (\epsilon_1 + 1)/\epsilon_m + (1-p)/\epsilon_1$; ω_{LOj} and ω_{TOj} are longitudinal and transverse mode phonon frequencies for CdS and CdSe. ϵ_m is the dielectric constant of the medium, mercaptoacetic acid in our case. The theory of electron-phonon interaction shows that SP modes with $l=1$ and those with l =even can contribute to Raman scattering via the deformation potential of electron-phonon interaction [31, 32] or the Frohlich electron-phonon coupling [33], respectively. The higher SP modes ($l > 2$) contribute only slightly to the scattering intensity. Thus, we can assign the surface modes only with $l=2$. As before, we have taken the values of ω_{LO1} and ω_{LO2} as 302 cm^{-1} and 213 cm^{-1} and the values of ω_{TO1} and ω_{TO2} as 238 cm^{-1} and 168 cm^{-1} , respectively. The values of other parameters are $\epsilon_m = 14.3$, $\epsilon_1 = 5.5$ and $\epsilon_2 = 8.9$ [34]. The average value of t is known from HRTEM and Raman measurements to be 1.2 nm. The solid line and the dashed line in Fig. 8 shows the variation of CdS-like and CdSe-like SP frequencies with x for $l=2$ using Eqn. 11. The observed values of CdS-like and CdSe like SP frequencies in Sample B are shown as filled circles in Fig. 8. These values correspond to $x=1.8$.

We have observed that the SP mode for Sample A at 183 cm^{-1} , which is very close to the value of ω_{SP} (182 cm^{-1}) for pure CdSe particles, obtained from Eqn. 10. On the other hand, the observed CdS-like SP frequency (244 cm^{-1}) from the shell component of the Sample B is away from the frequency (252 cm^{-1}) of the same for pure CdS particles, estimated directly from Eqn. 10 or with $x=0$ ($p=1$) in Eqn. 11 (shown by filled square in Fig. 8). However, it is close to the value, 243 cm^{-1} , obtained from Eqn. 12 with $x=1.8$

Sam ple	$\omega_{SP\ CdSe\ (calc)}$	$\omega_{SP\ CdSe\ (expt)}$	$\omega_{SP\ CdS\ (calc)}$	$\omega_{SP\ CdS\ (expt)}$
Sam ple A	182	183	–	–
Sam ple B	177	180	243	244

TABLE IV : Calculated and experimental CdS and CdSe-like SP frequencies in Sample A and B . The unit for above frequencies are in cm^{-1}

using dielectric response function model for two oscillators. The corresponding CdSe-like mode in Sample B is expected to appear at 176 cm^{-1} . The mismatch between this estimated value and observed frequency of SP mode (180 cm^{-1}) for the core material may be due to the effect of interface between core and shell structure. The SP frequencies for the CdS-like and CdSe-like modes in Sample A and B as obtained from the experiments and above calculations are tabulated in Table IV .

It is interesting to note that if CdSe-CdS would form a mixed crystal in the solution, we expect (from detailed theory of SP modes in mixed crystals) CdSe-like and CdS-like SP modes for sample B to appear at 204 cm^{-1} and 267 cm^{-1} , respectively [19]. This is far away from what we have got experimentally. Thus, the above discussion implies that from the SP frequencies of the expected shell material, one can confirm the formation of core-shell like particle, rather than formation of mixed nanocrystallites or individual particle of shell material in the sample.

V I. C O N C L U S I O N

Our goal in this article was to show electron and phonon confinement in the CdSe-CdS core-shell nanostructure. To this end, we have first confirmed the existence of the core-shell structure in our samples, prepared by soft chemical route, using HRTEM images. Subsequently, to analyze the electronic transitions we focus on optical absorption measurements, supported by theoretical considerations of the effective bond order model. Furthermore, the first order Raman line shape of the CdSe-CdS nanocrystals is quantitatively explained by taking into account both confined phonon modes and SP modes. The frequencies of SP modes are shown to match well with their calculated values as obtained from the dielectric response function model. We also demonstrate that due to passivated surface states CdS capped samples exhibit clear SP modes separated from LO modes in core-shell type

nanocrystallites. In summary, we have presented a technique to confirm the core-shell structure in this type of semiconductor nanostructure.

While analysing the optical absorption of the CdSe-CdS core-shell structure using effective bond order model, we have assumed the expected electronic transitions for CdSe and CdS particles. The phonon confinement in the shell structure is explained by taking the shell as a thin layer on CdSe core. The above assumptions may or may not play a crucial role in analyzing the data. However, more accurate theoretical models are necessary to understand core-shell structure better.

VII. ACKNOWLEDGEMENT

AR thanks DST and BRNS in India, for financial support.

-
- [1] Nanoparticles From theory and application Ed. Gunter Schmid Wiley-VCH Verlag GmbH & Co. KGaA, Weinheim, 2004 and the references therein.
 - [2] L. Spanhel, M. Haase, H. Weller and A. Henglein, J. Am. Chem. Soc. 109, 5649 (1987).
 - [3] D. Dorfs and A. Eychmüller, Nano Lett. 1, 663 (2001).
 - [4] X. Peng, M. C. Schlamp, A. V. Kadavanich and A. P. Alivisatos, J. Am. Chem. Soc. 119, 7019 (1997).
 - [5] W. L. Wilson, P. J. Sza jowski, L. E. Brus, Science 262, 1242 (1993).
 - [6] A. R. Kortan, R. Hull, R. L. Opila, M. G. Bawendi, M. L. Steigerwald, P. J. Carroll, L. E. Brus J. Am. Chem. Soc. 112, 1327 (1990).
 - [7] C. F. Hoener, K. A. Allan, A. J. Bard, A. Champion, M. A. Fox, T. E. Mallouk, S. E. Webber and J. M. White, J. Phys. Chem. 96, 3812 (1992).
 - [8] A. Mews, A. Eychmüller, M. Giersig, D. Schooss, and H. J. Weller, Phys. Chem. 98, 934 (1994).
 - [9] M. Danek, K. F. Jensen, B. C. Murray, and G. M. Bawendi, Chem. Mater. 8, 173 (1996).
 - [10] M. A. Hines, and P. G. Sionnest, J. Phys. Chem. 100, 468 (1996).
 - [11] N. Pradhan, B. Katz and S. Efrima, J. Phys. Chem. B 107, 13843 (2003).
 - [12] M. Danek, K. F. Jensen, C. B. Murray, M. G. Bawendi Appl. Phys. Lett. 65, 2795 (1994).
 - [13] I. H. Campbell and P. M. Fauchet, Solid State Commun. 58, 739 (1986).

- [14] H. Richter, Z.P. Wang and L. Ley, Solid State Commun. 39, 625 (1981).
- [15] R.J. Nemanich, S.A. Solin and R.M. Martin, Phys. Rev. B 23, 6348 (1981).
- [16] R. Tsu, H. Shen and M. Dutta, Appl. Phys. Lett. 16, 112 (1992).
- [17] A.K. Sood, K. Jayaram and D.V.S. Muthu, J. Appl. Phys. 72, 4963 (1992).
- [18] A. Roy, K. Jayaram and A.K. Sood, Solid State Commun. 89, 229 (1994).
- [19] A. Roy and A.K. Sood, Phys. Rev. B 53, 12127 (1996).
- [20] R. Fuchs and K.L. Klier, J. Opt. Soc. Am 58, 319 (1968).
- [21] A.V. Baranov, Yu.P. Rakovich, J.F. Donegan, T.S. Perova, R.A. Moore, D.V. Talapin, A.L. Rogach, Y. Masumoto and I. Nabiev, Phys. Rev. B 68, 165306 (2003).
- [22] D.J. Norris, A. Scara, C.B. Murray, M.G. Bawendi, Phys. Rev. Lett. 72, 2612 (1994).
- [23] W. Hoheisel, V.L. Colvin, C.S. Johnson and A.P. Alivisatos, J. Chem. Phys. 101, 8455 (1994).
- [24] J. Nanda, B.A. Kuruvilla, and D.D. Sama, Phys. Rev. B 59, 7473 (1999).
- [25] S.M. Liu, H. Guo, Z.-H. Zhang, R. Li, W. Chen and Z.-G. Wang Physica E 8 174 (2000).
- [26] X-ray Powder Diffraction, JCPDS file.
- [27] L.M. Ramaniah, and S.V. Nair, Phys. Rev. B 47, 7132 (1993).
- [28] M. Nirmal, D.J. Norris, M. Kuno and M.G. Bawendi, Phys. Rev. Lett. 75, 3728 (1995).
- [29] C. Trallero-Giner, A. Debemardi, M. Cardona, E. Menendez Proupin, A.I. Ekimov, Phys. Rev. B 57, 4664 (1998).
- [30] H. Bliz and W. Kress, Phonon dispersion relations in insulators (Springer Verlag, p. 97, 1979); also see Reference [2] p.63 & p.143.
- [31] R. Ruppin, R. Englman, Rep. Prog. Phys. 33, 146 (1970).
- [32] A.V. Fedorov, A.V. Baranov, K. Inoue, Phys. Rev. B 56, 7491 (1997).
- [33] F. Comas, C. Trallero-Giner, N. Studart and G.E. Marques, Phys. Rev. B 65 073303 (2002).
- [34] Handbook of Chemistry and Physics, David R. Lide, Ed. in Chief, CRC Press.

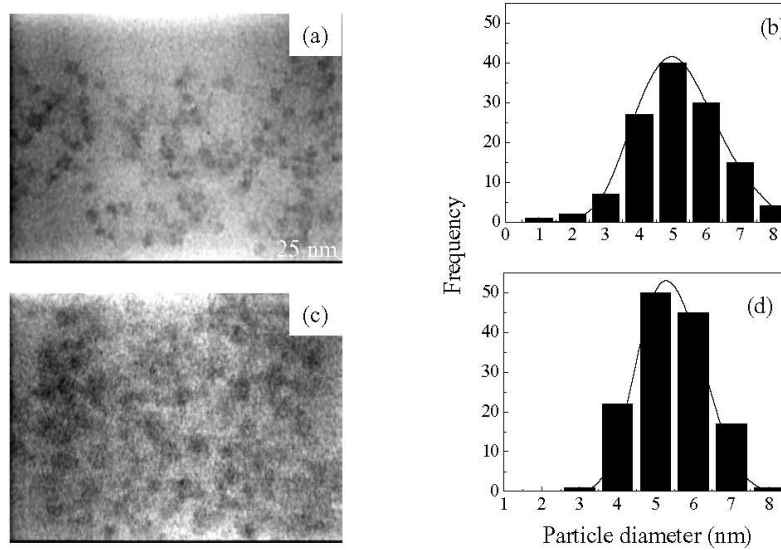


FIG .2: Low magnification micrographs and histogram of the nanocrystals. (a) is the TEM micrograph and (b) is the corresponding histogram for Samples A. Similarly, (c) is the micrograph and (d) is the corresponding histogram for Sample B.

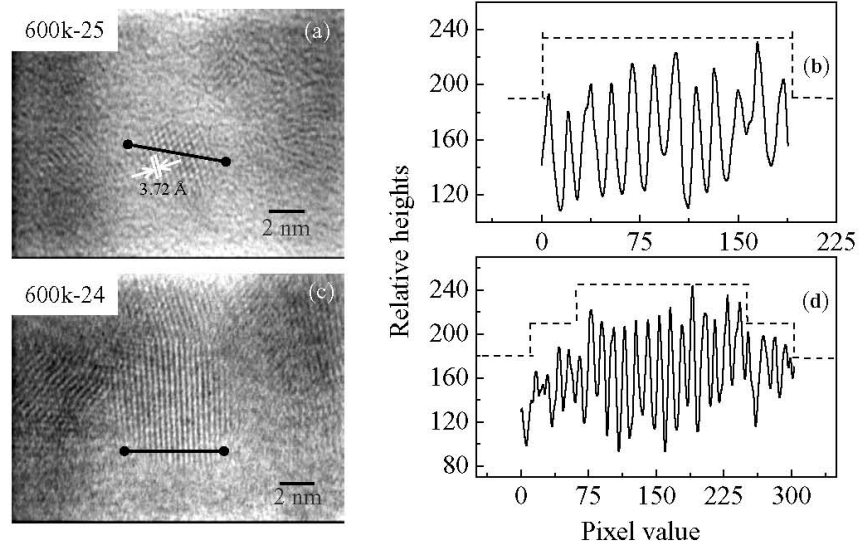


FIG . 3: High resolution TEM micrographs and corresponding line profiles for Sample A and B .

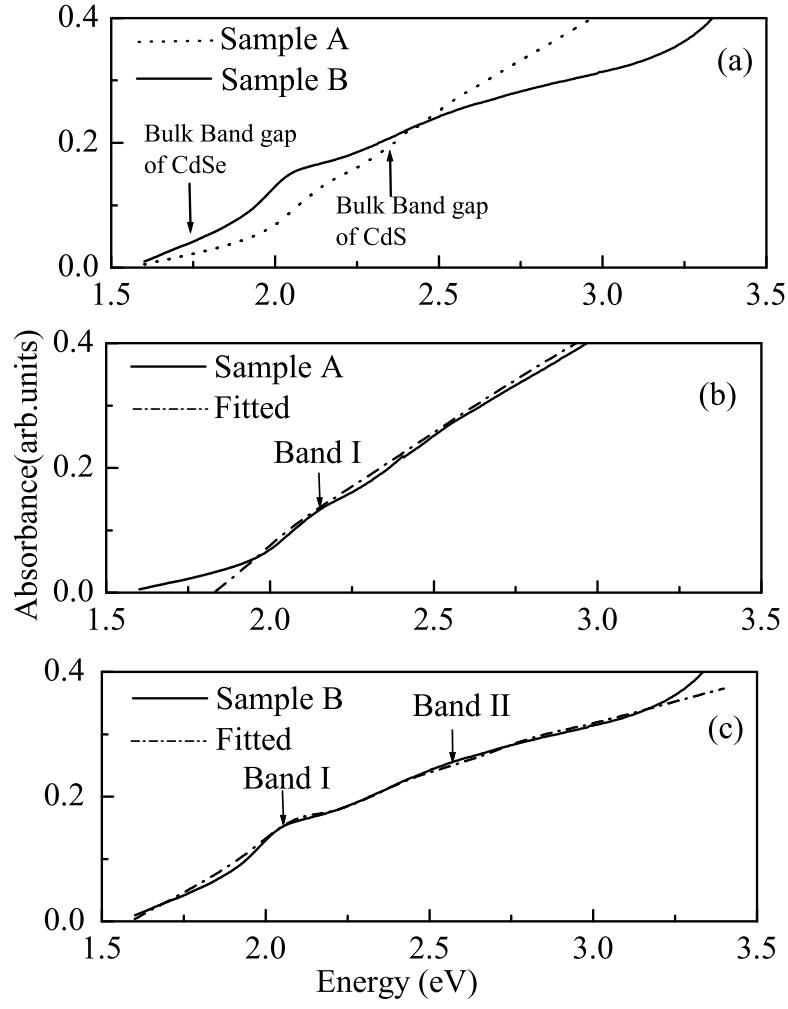


FIG . 4: (a) Optical absorption spectra for Sample A and B. The dotted line is the spectrum for CdSe particles and solid line is for CdSe-CdS core-shell particles. The bulk band gap positions for CdS and CdSe are shown by arrows. (b) and (c) The dashed dotted lines are the nonlinear least square fit to the experimental curves (solid lines) using effective bond order model.

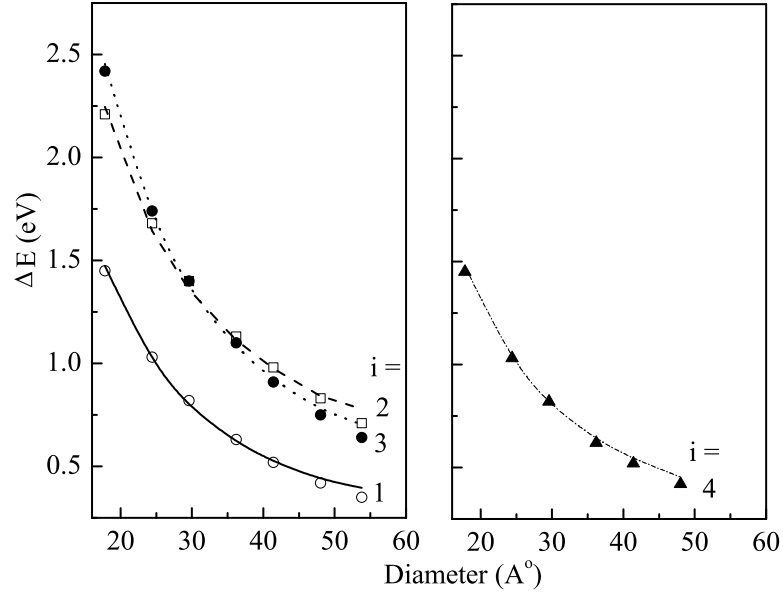


FIG . 5: The variation in ΔE with respect to diameter, d , of the particle for different transitions in effective bond order model for CdSe and CdS. The curve through the points are fit to $E = A_i d^{-x_i}$.

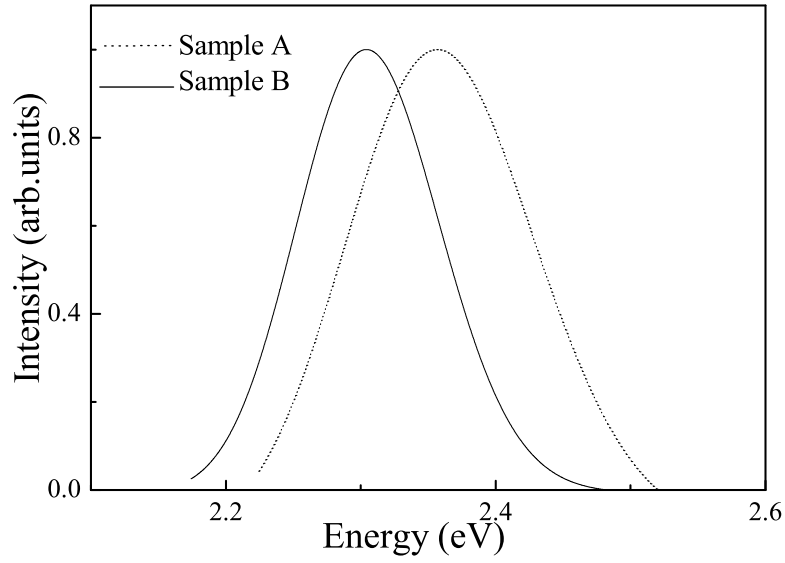


FIG . 6: PL spectra for Sample A and B .

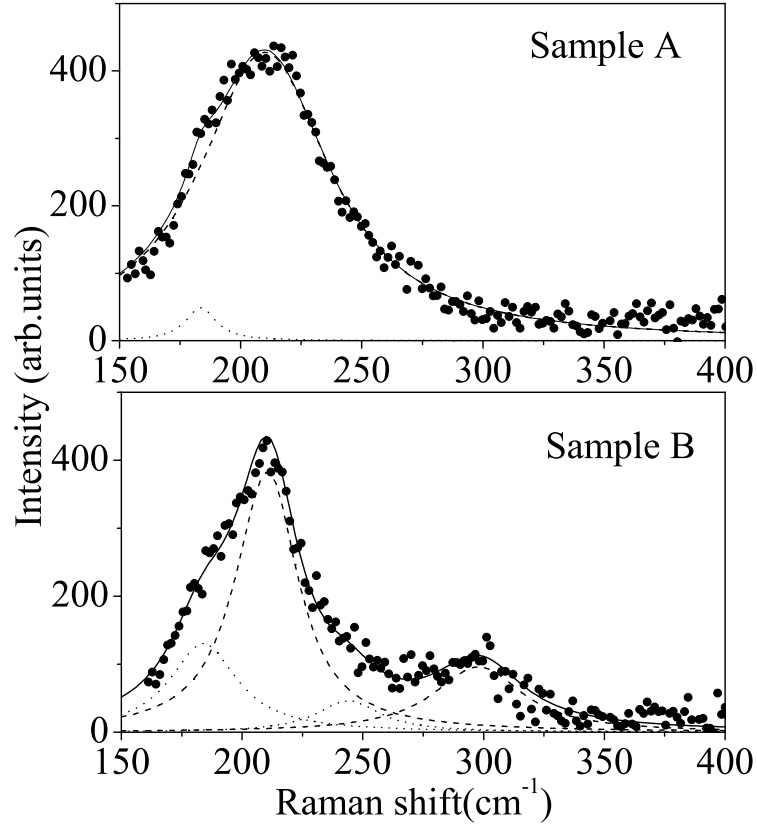


FIG. 7: Raman spectra for Sample A and Sample B are shown by filled circles. Phonon component and surface phonon components are given by dashed and dotted lines, respectively. Solid lines correspond to the best fit to the experimental data using combined Raman line shapes

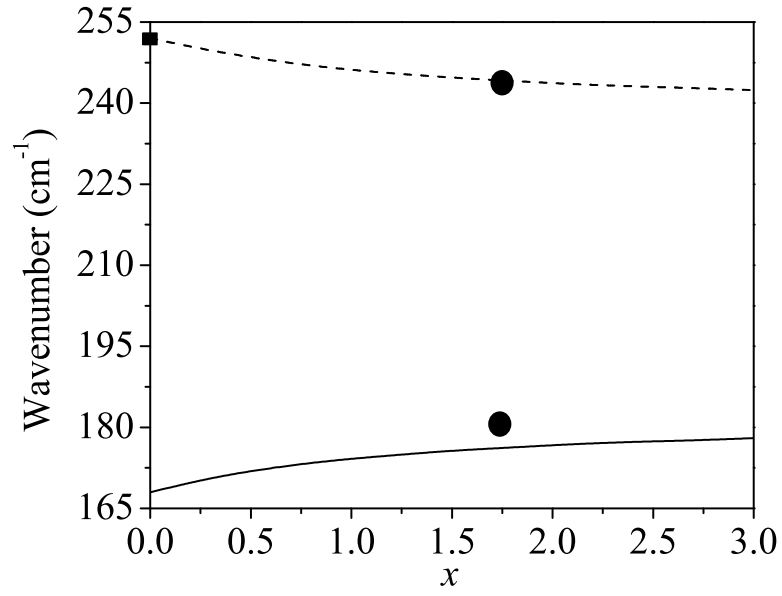


FIG .8: Variation of CdS like (dashed line) and CdSe like (solid line) SP phonon frequencies with x . The solid circles are SP frequencies for the Sample B. The solid square is the estimated SP frequency in pure CdS nanoparticle [$x=0$; $p=1$]